Local Moment Instability of Os in Honeycomb $Li_{2.15}Os_{0.85}O_3$

M. K. Wallace[1], P. G. LaBarre[2], Jun Li[1], S.-T. Pi[3], W. E. Pickett[3], D.S. Dessau[4], D. Haskel[5], A. P. Ramirez[2], M. A. Subramanian[1]

[1]*Department of Chemistry, Oregon State University, Corvallis, OR 97331*
[2] *Department of Physics, University of California, Santa Cruz, Santa Cruz, CA 95064*
[3] *Department of Physics, University of California Davis, Davis, CA 95616*
[4] *Department of Physics, University of Colorado, CO 80309*
[5]*Advanced Photon Source, Argonne National Laboratory, Argonne IL 60439*

Abstract

Compounds with honeycomb structures occupied by large spin orbit coupled (SOC) moments are considered to be candidate Kitaev quantum spin liquids. Here we present the first example of Os on a honeycomb structure, $Li_{2.15(3)}Os_{0.85(3)}O_3$. This compound is an off-stoichiometric version of Li_2OsO_3 with the beta-Li_2SnO_3 structure ($C2/c$) ($a = 5.09$ Å, $b = 8.81$ Å, $c = 9.83$ Å, $\beta = 99.3º$). Neutron diffraction shows large site disorder in the honeycomb layer and X-ray absorption spectroscopy indicates a valence state of Os ($+4.7 \pm 0.2$), consistent with the nominal concentration. We observe a narrow transport band gap of $\Delta = 243 \pm 23$ meV, a large van Vleck susceptibility, and an effective moment of 0.85 μ_B, much lower than expected from 70% Os(+5). No evidence of long range order is found above 0.10 K but a spin glass-like peak in ac-susceptibility is observed at 0.5 K. The specific heat displays an impurity spin contribution in addition to a power law $\propto T^{0.63 \pm 0.06}$. Density functional theory (DFT) applied to Li_2OsO_3 leads to a reduced moment, suggesting incipient itineracy of the valence electrons. Constrained non-collinear moment DFT is applied to an ordered version of $Li_{2.25}Os_{0.75}O_3$, finding evidence that Li over stoichiometry leads to Os(4+)-Os(5+) mixed valence. This local picture is discussed in light of the site disorder and a possible underlying quantum spin liquid state.

Introduction

The demonstration by Kitaev of an exactly solvable quantum spin liquid (QSL) model incorporating S = ½ spins with anisotropic interactions on a honeycomb lattice [1,2] has motivated searches for its experimental realization. Whereas magnetic honeycomb-containing

compounds have been extensively investigated in $3d$ and $4d$ metal oxides [3-11], the strong interaction anisotropy required by Kitaev's theory has placed a focus on $5d$ metal oxides, for which strong spin-orbit coupling (SOC), the origin of spatial anisotropy, can be expected [12-18]. In the A_2MO_3 honeycomb structure, where A is an alkali element and M a $4d$ or $5d$ element, the AM_2 layers form a hexagonal network of edge sharing MO_6 octahedra with a single A^+ ion at the centers of the hexagons (Figure 1). Examples such as α-Na_2IrO_3 and α-Li_2IrO_3 with effective spin $J_{eff} = \frac{1}{2}$, have recently emerged as possible examples of Kitaev physics. These compounds possess antiferromagnetic (AF) Weiss temperatures of 125(6) K and 33(3) K and undergo AF order at 15.5 K and 14.5 K for Na_2IrO_3 and Li_2IrO_3 respectively [19,20]. The 3D hyper-honeycomb lattice compound β-Li_2IrO_3, however, demonstrates a ferromagnetic (FM) Weiss temperature of 40 K and weak ordering signatures at 38 K among $J_{eff} = \frac{1}{2}$ moments [21]. Among non-oxide materials, the layered compound α-$RuCl_3$ has also been discussed as a possible Kitaev system, though it too undergoes long range order at 7.5 K [22]. Since the suppression of classical order via geometrical frustration is a requirement for creating a QSL state, the above systems, while possessing important attributes, fall short of the Kitaev criteria [23]. Thus, it is important to study other honeycomb-containing compounds with the potential for optimizing the microscopic energy scales.

Given the importance of SOC for establishing a Kitaev state on a honeycomb structure, we ask here what would be the result of *reducing* the SOC from that of 540 meV in Ir to 480 meV in Os [24]. In the present work we report on the synthesis, structure, and properties of $Li_{2.15(3)}Os_{0.85(3)}O_3$ which is isostructural to the Ir honeycomb compounds mentioned above. For the stoichiometric compound, Li_2OsO_3, the Os ion is expected to be in the $4+ = d^4$, $J_{eff} = 0$ state to maintain charge-neutrality. In our work, we find that, for each crystallographic site

representing the $LiOs_2$ layer, an average of 43% of the sites (compared to the expected 33% of these sites) are occupied by lithium and thus the average valence of Os is $+4.5 \pm 0.1$ ($\sim d^{3.5}$), a value consistent with our X-ray absorption spectroscopy (XAS) measurements, which yield $+4.7 \pm 0.2$. From a local moment perspective and using the XAS-determined valence state, our system might be comprised of 30% d^4 ($J_{eff} = 0$) and 70% d^5 ($J_{eff} = 3/2$) but its physical properties are not easily understood. We find a transport gap of 243 meV, an effective magnetic moment of 0.85 μ_B, which is much less than the effective moment of 3.24 μ_B expected if 70% of the ions possessed $J_{eff} = 3/2$. No magnetic order is observed above 0.10 K, and the specific heat obeys a fractional power law in temperature and is only weakly magnetic field-dependent. We discuss the constraints on the local physics of Os from a band structure perspective and their implications for collective behavior en route to a possible QSL in SOC honeycomb systems.

Experimental

Stoichiometric amounts of Li_2CO_3 and OsO_2 (synthesized from osmium metal) were intimately ground, pressed into a pellet, loaded into an alumina crucible, and fired in a tube furnace at 700 C under Argon flow. Firing was repeated to 850 C with 50 C increments, grinding the sample before each firing. Each firing was performed under argon flow. Phase analysis of the powder samples was performed by X-ray diffraction using a Rigaku MiniFlex II diffractometer with Cu Kα radiation and a graphite monochromator for the diffracted beam. Time of Flight (TOF) neutron diffraction measurements were collected at Oak Ridge National Laboratory NOMAD BL-1B SNS beamline. X-ray absorption spectroscopy measurements were carried out at beamline 4-ID-D of the Advanced Photon Source at Argonne National Laboratory using a transmission geometry. Reference samples for valence determination included Os metal, $Os^{4+}O_2$ and $Sr_2FeOs^{5+}O_6$ [25]. The Seebeck coefficient and electrical conductivity data (350 K – 600 K)

were collected on an ULVACRIKO ZEM-3 under a helium atmosphere. Magnetization measurements (2 K - 300 K) were obtained with a Quantum Design MPMS. Resistivity, $\rho(T)$, (200 K - 350 K) and specific heat, $C(T)$, data (2 K -30 K) were obtained using a Quantum Design PPMS. Magnetic ac-susceptibility data down to 0.1 K were obtained in a ^{3}He-^{4}He dilution refrigerator with thermal contact to the mixing chamber made via a copper wire bundle bonded to the sample with Stycast 1266 epoxy. Data were obtained at 143 Hz and with an excitation current low enough to eliminate heating from the coils.

Crystal Structure

Common space groups assigned to honeycomb-structure compound Li_2MO_3 (M = Mo, Mn, Rh, Ir, Ru, Pt, and Sn) are $C2/m$, $C2/c$, and $R\overline{3}m$ [4,7-9,17,26-33]. Figure S1 represents Li_2MO_3 $C2/m$, $C2/c$, and $R\overline{3}m$ unit cells illustrated down the b-axis (top) and corresponding portion of the Li-M layer representing a single hexagon configuration (bottom) with lithium and metal occupying their ideal Wyckoff positions [4,17,29,30,33]. For all three space groups, edge sharing octahedral LiM_2 layers alternate with edge sharing octahedral Li layers. The difference in space groups and their associated symmetries can in part be ascribed to stacking of the LiM_2 layers, with $R\overline{3}m$ as the highest in symmetry. The space group assignments of some Li_2MO_3 systems has been controversial. For example, Li_2MnO_3 was first refined to be $C2/c$, but later found to be $C2/m$ on the basis of electron diffraction and transmission electron microscopy [27,28]. Another example is Li_2MoO_3, which was reported as both $C2/c$ and $R\overline{3}m$ [4,29]. When comparing literature on polycrystalline Li_2IrO_3 synthesized under standard solid state conditions, discrepancies in $C2/c$ and $C2/m$ space groups exist. Recent work supports the higher symmetry $C2/m$ as the appropriate space group for polycrystalline Li_2IrO_3 [17,30,33]. The powder X-ray diffraction pattern of Li_2OsO_3 is shown in Figure 2. At first glance, the X-ray pattern pointed to a

more symmetric space group, $R\bar{3}m$, however, close examination of the pattern showed weak and broad diffraction peaks in the 2θ region of 19° to 33°. It is known that for both $C2/m$ and $C2/c$ systems, with no Li-M site exchange within the LiM_2 layers, sharp peaks exist within the 19° to 33° range. However, introducing Li-M site exchange within the LiM_2 layers decreases the relative intensities of these peaks, leading to virtually no peak presence at ~30% Li-M site exchange [31]. Such a reduction in diffraction peak intensity is also found for (hk0) reflections past 38° [31]. Disorder among Li-M sites is commonly reported for honeycomb layered metal oxides since all corresponding crystallographic sites are octahedral and similar in size [4,9,17,18,27-29]. The presence of stacking faults associated with a shift between successive LiM_2 layers will cause the peaks in the region from 19° to 33° to further broaden asymmetrically [7-9,18]. Thus, with the existence of Li-M site disorder and stacking faults, it is difficult to distinguish between the corresponding space groups using powder X-ray diffraction. The x-ray scattering length for lithium and oxygen are also small due to their low Z. Because of the neutron scattering lengths of lithium, osmium, and oxygen, neutron diffraction is ideal to characterize the Li_2OsO_3 structure. To determine the crystal structure, Rietveld refinements were performed on room temperature neutron diffraction data using the GSAS program (Figure 3). The current synthesis procedure restricted diffraction measurements to the Oak Ridge NOMAD TOF Neutron beamline, which is well-suited for small sample sizes. A pseudo-Voigt peak shape profile was chosen and parameters refined to obtain the best fit to the collected data. The space group was refined to be $C2/c$, with lattice dimensions a = 5.09 Å, b = 8.81 Å, c = 9.83 Å, and β= 99.3°. Rietveld refinements for all collected banks are shown in Figure S2, with cumulative wRp = 6.40% and χ^2 = 4.8. The atomic coordinates, occupancies, and isotropic displacement parameters are represented in Table 1. Interatomic distances and angles are given in Table S1.

No osmium is detected in the lithium-only layers. For *C2/c* there are three unique atomic positions to describe the Li and Os sites within the $LiOs_2$ layer (Figure S3). Shown in Table 1, corresponding sites are labeled as Li/Os 3, 4, and 5. If no Li-Os site disorder existed within the $LiOs_2$ layer, only Li3, Os4, and Os5 would exist (each with an occupancy of 1), with Os4 and Os5 sites describing the honeycomb rings. As shown from Table 1 occupancies, a large percentage of Li-Os site disorder exists within the $LiOs_2$ layer. For each of the three respective crystallographic sites, an average of 43% is occupied by lithium. The stoichiometry derived from occupancy refinements of Li, Os, and O is $Li_{2.15(3)}Os_{0.85(3)}O_3$ suggesting an average osmium oxidation state of 4.5± 0.1. It is important to note that oxygen occupancy refinements indicate that the oxygen sites are fully occupied and no detectable vacancies are observed. Though 2:1 stoichiometric amounts of Li:Os were used in the synthesis, the refined stoichiometric ratio is considered reasonable as the presence of a small amount of osmium impurity is formed during the synthesis and was removed by heating the sample in air at 300 ^{0}C as OsO_4 through sublimation. Stacking faults were modeled using the DIFFaX program and the description of the model and analogous XRD patterns are discussed in the SI section. From the discussion presented, the absence of the (020) peak can only be attributed to Li-Os site disorder within the $LiOs_2$ layers and not from stacking faults, consistent with the neutron refinement.

XAS measurements at the Os $L_{2,3}$ absorption edges (Figure 4) were used to provide an additional estimate of Os valence. The enhanced x-ray absorption above the leading edge ("white line") is a result of large density of empty 5d states near the Fermi level. This peak grows in intensity and shifts to higher energy with increasing Os oxidation state. Interpolating the XAS peak position in the honeycomb sample onto those of the reference compounds yields an oxidation state of +4.7 ± 0.2, within errors of results from structure refinements. The ratio of L_3

to L_2 white line intensity, also known as the isotropic branching ratio (BR), provides a measure of the relevance of SOC interactions in the 5d band [34,35]. In the absence of sizable SOC interactions, the isotropic branching ratio equals 2 reflecting the different occupancies of the core levels at L_3 and L_2 edges. We measured BR=2.9(1) which significantly differs from the statistical value of 2 and indicates that SOC interactions need to be included in order to describe the 5d electronic structure of this compound.

Thermodynamic and Transport Properties

Temperature dependent resistivity and Seebeck measurements from 300 – 600 Kelvin are shown in Figures 5 and 6. The gap energy (E_g) for the sample was extracted using $\rho = \rho_0 \exp(E_g/2k_BT)$ with E_g = 220 meV and 266 meV obtained from low- and high-temperature transport measurements respectively, thus indicating a small band gap insulator (Figure 6 b).

The magnetic susceptibility, χ_{dc}, for H = 0.5 T (Figure 7) suggests the combined effects of Curie-Weiss as well as van Vleck temperature independent paramagnetism over the entire measurement range above 2 K. Within this assumption, we varied the magnitude of the van Vleck term, χ_{VV}, to produce a pure Curie-Weiss contribution. We found that subtracting χ_{VV} = 0.00135 emu/mole from the measured $\chi(T)$ produces the straightest $1/\chi(T)$, resulting in a good fit to the Curie-Weiss form, $\chi = C/(T-\theta)$, where C is the Curie constant and, θ is the Weiss constant. Fitting the data between 50 and 200 K yields a Weiss constant of θ = -11.5 K and a finite effective moment μ_{eff} = 0.85 μ_B, significantly *greater* than expected for the J_{eff} = 0 state of Os(+4). Given the above XAS and neutron scattering refinement results showing that the average Os valence is 4.7, however, an alternate ionic scenario is for 70% of the Os ions to be in the +5 state (J_{eff} = 3/2) and 30% in the +4 state (J_{eff} = 0). This analysis yields μ_{eff} = 1.01 μ_B (θ = -11.8 K) for the magnetic (+5) ions, which is now significantly *less* than the expected moment. We

discuss possible sources of this discrepancy below.

These χ_{dc} data were augmented with ac-susceptibility (χ_{ac}) data down to 0.1 K, which were calibrated to the χ_{dc} data in the overlapping temperature range 2.0 – 2.5 K. A peak in χ_{ac} is observed at 0.5 K, but is rapidly suppressed by magnetic fields far less than 0.1T. Given the usual relationship between H and T for a g-factor of two, one expects suppression of an antiferromagnetic ordering feature at 0.5 K for H values an order of magnitude larger than observed. Alternatively, such a cusp in χ_{ac} can be attributed to spin glass freezing, a scenario consistent with the high degree of disorder in this spin system. The spins involved in such freezing may not represent the bulk of the Os(+5) spin population, as we argue below.

The existence of a small subset of spins that are interacting at a mean field energy scale of k_BT for T = 0.5 K, as suggested by the χ_{ac} peak, is also supported by $C(T,H)$, shown in Figure 8. Here, C/T exhibits an upturn below its minimum at T = 6 K. This upturn is only moderately affected by fields up to 8 T, so we model this as $C = C_1(T) + C_2(T,H)$. Here C_1 is a combination of the lattice specific heat and an H-independent electronic contribution. Taking the difference between $C(H = 8T)$ and $C(H = 0)$, we find that $C_2(T,H=8T)$ resembles a broadened Schottky anomaly (Figure 8 upper inset). We can fit this contribution to either a single J_{eff} = 3/2 (g = 1.3) Schottky anomaly or a pair of J_{eff} = ½ (g = 2.6 and 7.4) Schottky anomalies with molar concentrations of 4.1% and 9.6% (total for the pair) respectively. (Assuming 70% of the spins are magnetic, these fractions become 5.9% and 13.7%). Thus, it is not unlikely that the spins undergoing spin-glass-like freezing are the same spins responsible for the Curie-tail susceptibility. We now turn to the $C_1(T)$ term, which is calculated using the two different Schottky approximations mentioned above and plotted in the lower inset of Figure 8. We note that, below 8 K, $C_1(T) \propto T^{\alpha}$, where α = 0.69 and 0.57 for the J_{eff} = 3/2 and 1/2 Schottky analyses respectively.

Such a sublinear form cannot persist down to the lowest temperatures, and importantly is clearly distinct from the phonon contribution visible above 8 K. At the same time, it appears that, among the 70% of Os ions that are in a +5 state (within an ionic picture) and thus possibly magnetic, less than ~15% are accounted for in either susceptibility or field-dependent specific heat. If the sublinear low-T contribution is due to these unaccounted for, but nevertheless magnetic, Os(+5) ions, then they must be in a type of singlet state due to exchange interactions with a strength greater than the Zeeman energy of an 8 Tesla field, but of a type that invalidates the effective moment approximation below room temperature.

Electronic Structure and Magnetism

Early model treatments of $5d$ oxides on honeycomb lattices built on the ionic description of crystal field splitting, additionally with strong SOC among orbitals, focused attention on the t_{2g} subshell $J_{eff} = 1/2$ and $3/2$ subspaces. The relevant energy scales of individual bandwidth W, Hubbard U, Hund's J_H, and SOC strength ξ, all lie in the 0.5-1.5 eV range, and studies of the electronic structure and especially the exchange coupling have concluded that the ionic picture provides a challenging starting point at best. The electronic structure of octahedral osmates is complicated by two overriding features. First, the active t_{2g} orbitals are strongly hybridized with the oxygen $2p\pi$ orbitals, resulting in strongly coupled Os $5d$ – O $2p$ states as the fundamental chemical unit. Osmates in the Ba_2NaOsO_6 family, for example, have half of the spin density residing on the O octahedron [36,37]. Iridates behave similarly, leading to their characterization as *molecular orbital* compounds, which can lead to longer range exchange coupling parameters compared to more localized moments [38]. Second, SOC also affects the electronic structure, creating both single-ion as well as exchange anisotropy, the relative effects of which are difficult to disentangle. Third, the distortion from ideal rhombohedral symmetry introduces band anti-

crossings that result in very narrow, ~0.3 eV, individual bandwidths and the likelihood of small gaps, as shown below. Several theoretical studies of honeycomb iridates have concluded that magnetic interactions beyond the Heisenberg-Kitaev model are important, suggesting a more itinerant picture of the electronic structure [39-45].

Many of the general findings for iridates carry over to osmates. Our compound presents the additional complication of Os possessing a nominal valence of +4.7, so one must consider a mixture of d^3 with d^4 ions. The ionic picture of d^4 begins with a non-magnetic $J_{eff}=0$ ion and for d^3 the ionic value is $J_{eff} = 3/2$, and the insulating nature suggests these different ionic states reside on distinct lattice sites, as opposed to the intermediate valence picture. In this ionic picture, the measured $\mu_{eff} = 0.85\mu_B$ is challenging to account for, as mentioned above, which leads us to consider the general question of moment formation in nearly itinerant systems.

We have applied density functional theory (DFT) methods including SOC, correlation effects, and a fixed atomic spin moment method in our study of Li_2OsO_3 (see Supplemental Information for the description). Without magnetism, SOC is strong enough to provide a pseudogap but no gap, within the Os t_{2g} bands. This SOC-driven separation is compromised by crystal subfield splittings, bandwidth effects, and anti-crossings arising from structural distortion away from rhombohedral symmetry leaving two inequivalent Os sites. The resulting band structure (not shown) is that of a very narrow, essentially zero (indirect) gap semiconductor. Due to the molecular orbital nature of the t_{2g} band complex, intra-atomic repulsion effects as treated by the Hubbard U repulsion are ineffective in opening a gap, for reasonable values of U (2 eV or less). Antiferromagnetic order tends to encourage gap opening, producing Os moments of ~0.3 μ_B.

To include in the modeling the effect of the observed Os moment, we have adopted the

constrained atomic moment method as implemented in the *abinit* code [46]. This method proceeds not by specifying a value for U for the Os 5d orbitals, but by fixing the spin moment by applying an intra-atomic Zeeman field determined self-consistently; both magnitude and direction can be specified separately for any atom. Magnitudes of 0.8 μ_B and 0.5 μ_B have been studied; the latter value represents the ordered component expected of a 0.8 μ_B local (C-W) moment. Bandgaps of 0.25 eV and larger were obtained, depending weakly on the imposed moment but strongly on the magnetic alignment (the larger ones were for AFM order). The resulting orbital moments are minor, only a few hundredths of 1 μ_B, independent of the chosen direction of spin. These results do not fit that of a Mott insulator: there is no robust local moment, and Hubbard U is not needed to open a gap and has little effect on the size of the gap.

Due to intermixing of Li on the Os honeycomb lattice, we have made an initial study of the effect of intermixing, by replacing 25% of the Os sublattice by Li while keeping the Li sublattice intact. The Os moments are fixed with magnitude 0.8 μ_B and oriented along separate (111) axes to mimic disordered moments. The resulting band structure, shown in Figure 9, illustrates the flat individual bands that arise, and that a very small gap exists or is imminent, depending on details of the calculations. The bands are not significantly different in appearance from those of Li_2OsO_3.

We now focus on the effect of Li substitution on the remaining Os ions. This 25% replacement results in three Os sites, denoted by Os[j] which has j Li neighbors, j=0, 1, or 2. The formal valences of Os in this $Li_2(Li_{1/4}Os_{3/4})O_3$ structure should average to 5+. The periodicity leaves Os[0]-Os[1] chains and comparatively isolated Os[2] ions, which in addition to two Li neighbors the Os neighbor is at a long Os-Os separation. The spectral distribution of Os[2] in Figure 9 is substantially different from the other two, more representative of a higher oxidation

state. While simple electron count indicates that Li substitution must oxidize some Os ions, having two Li neighbors strongly drives neighboring Os ions to a higher valence.

This modeling illustrates that the Os valence is sensitive not only to the total charge available, but also to the local environment. Different valence states carry different moments, and sensitivity to the local environment suggests that variation of exchange constants promotes a frustration of magnetic order. Note in Figure 9 that although the spectral distributions of 5d weight are somewhat different for Os[0] and Os[1], the difference is not characteristic of different valence states, while that of Os[2] is: less weight in the occupied bands. This implication then is that of two Os(4+) ions and one Os(5+) ion, with an average valence of 4.67 consistent with spectroscopic evidence on our samples. More of a specific nature cannot be concluded because the Os moments were constrained (to be equal), whereas those of different valence states would not be equal.

Summary

We have presented the first example of Os on a honeycomb structure, $Li_{2.15(3)}Os_{0.85(3)}O_3$, and have characterized it with atomic, structural, and magneto-thermal probes. The Os ions have an average valence state of +4.7 and large site disorder exists in the honeycomb layers. This compound is a narrow band gap semiconductor. The magnetic susceptibility and specific heat are not easily understood using a local moment picture, which suggests that the valence electrons are close to itineracy, consistent with our density functional theory calculations. These results strongly suggest that spin orbit coupling of Os is playing an important role in the collective electronic behavior of this honeycomb system, and that further studies of osmates on frustrating lattices are warranted.
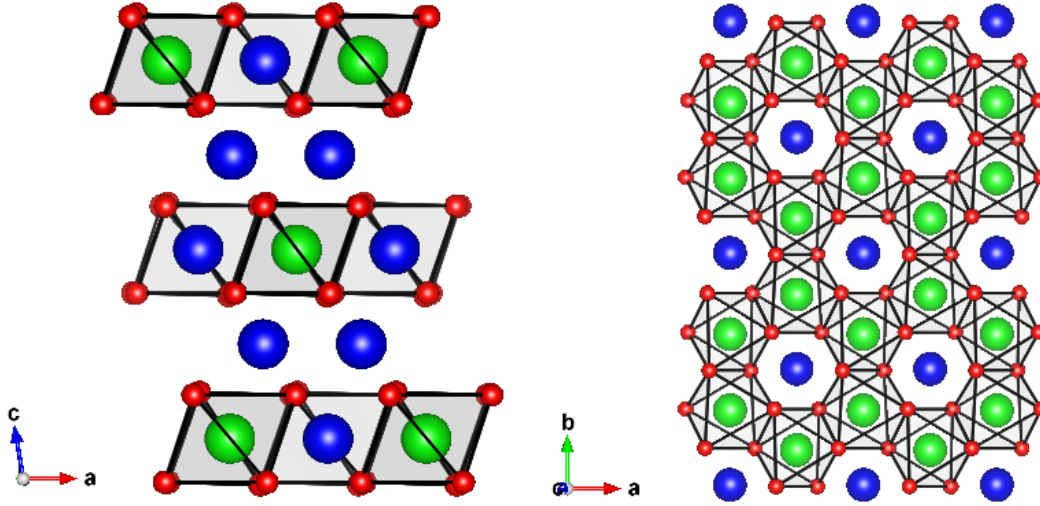
Acknowledgments

Figure 1. (a) Li_2MO_3 (M= 4d or 5d element) structure as alternating Li and LiM_2 layers and (b) viewed along the c axis the LiM_2 layer, where MO_6 edge-sharing octahedra form the honeycomb lattice. Blue, green, and red spheres represent lithium, metal, and oxygen atoms respectively.

Table 1. Atomic coordinates, occupancies and isotropic displacement parameters obtained from Rietveld refinement of TOF Neutron (Oak Ridge NOMAD BL-1B) diffraction data.

	Wyckoff	x	y	z	occ	U_{iso}
Li1	8f	0.2543(2)	0.0840(1)	0.0044(9)	1	0.25(8)
Li2	4d	0.25	0.25	0.5	1	0.037(4)
Li3	4e	0	0.7531(8)	0.25	0.32(4)	0.20(7)
Os3	4e	0	0.7531(8)	0.25	0.68(4)	0.20(7)
Os4	4e	0	0.0777(7)	0.25	0.46(2)	0.0043(2)
Li4	4e	0	0.0777(7)	0.25	0.54(2)	0.0043(2)
Os5	4e	0	0.4026(6)	0.25	0.56(2)	0.0082(2)
Li5	4e	0	0.4026(6)	0.25	0.44(2)	0.0082(2)
O1	8f	0.1335(7)	0.2414(5)	0.1344(4)	1	0.029(3)
O2	8f	0.1269(8)	0.5770(5)	0.1414(4)	1	0.0085(3)
O3	8f	0.1387(8)	0.9181(5)	0.1332(5)	1	0.0082(8)

Note: Cumulative wRp = 6.4% and χ^2 = 4.8. Stoichiometric identity is $Li_{2.15(3)}Os_{0.85(3)}O_3$
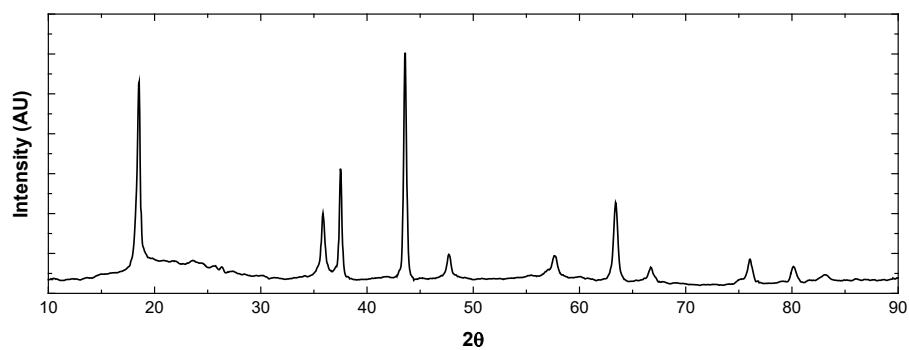
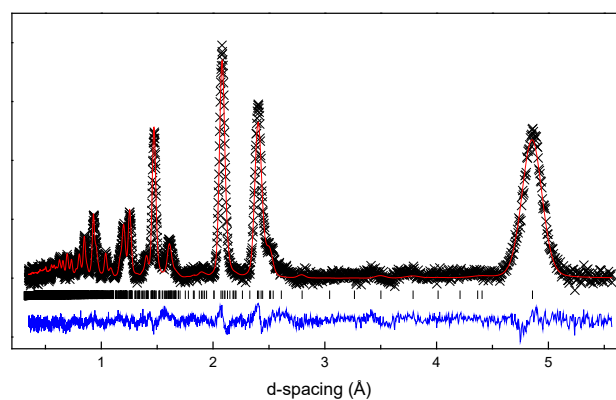**Figure 2.** XRD pattern of Li_2OsO_3 (λ= 1.514 Angstroms).

Figure 3. Rietveld refinement of TOF Neutron (Oak Ridge NOMAD BL-1B) diffraction data. The collected data (black cross), Rietveld refinement (red line), and difference (blue line) are presented for one of the four collected banks. Resulting cumulative residual factors are wRp = 6.4% and χ^2 = 4.8.
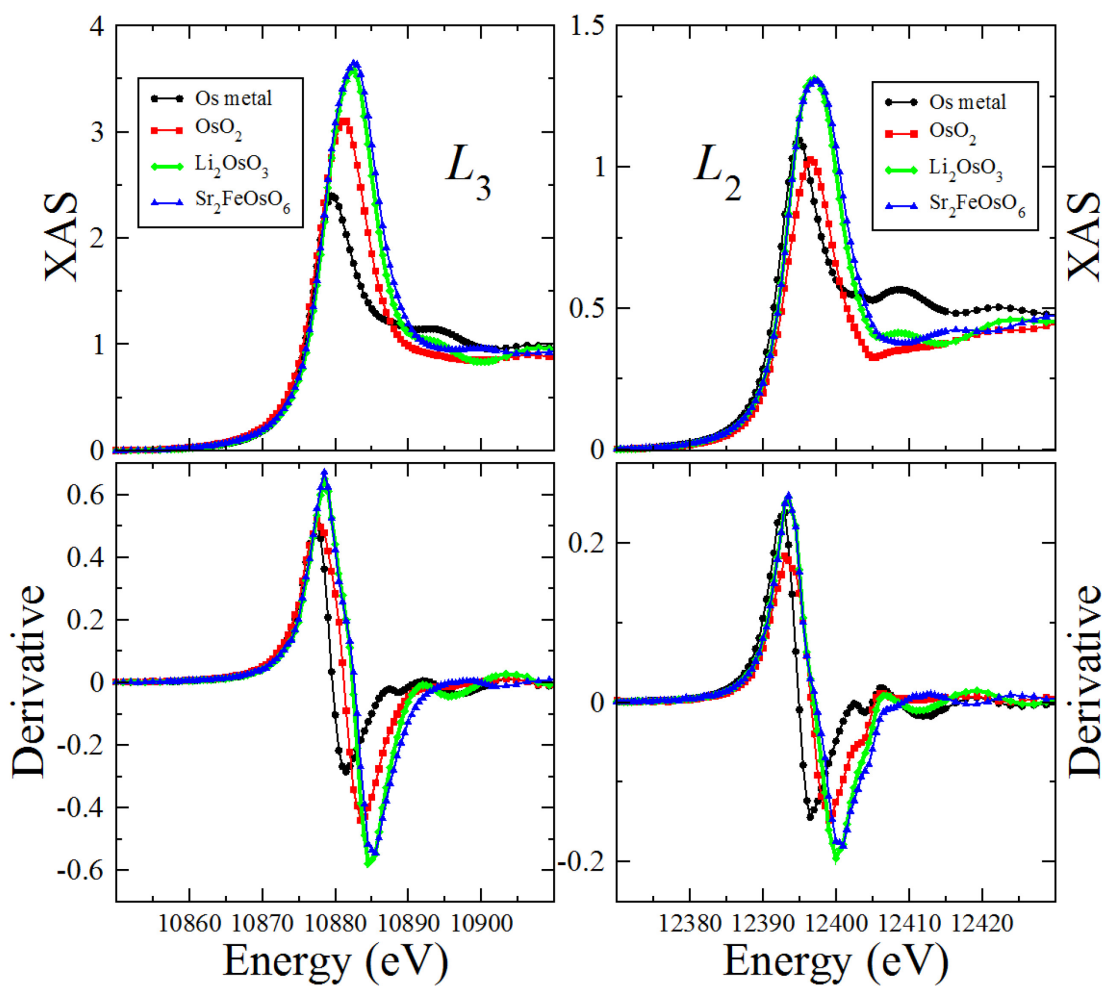
Figure 4. Os $L_{2,3}$ XAS measurements on $Li_{2.15}Os_{0.85}O_3$ and three reference compounds with known oxidation state.
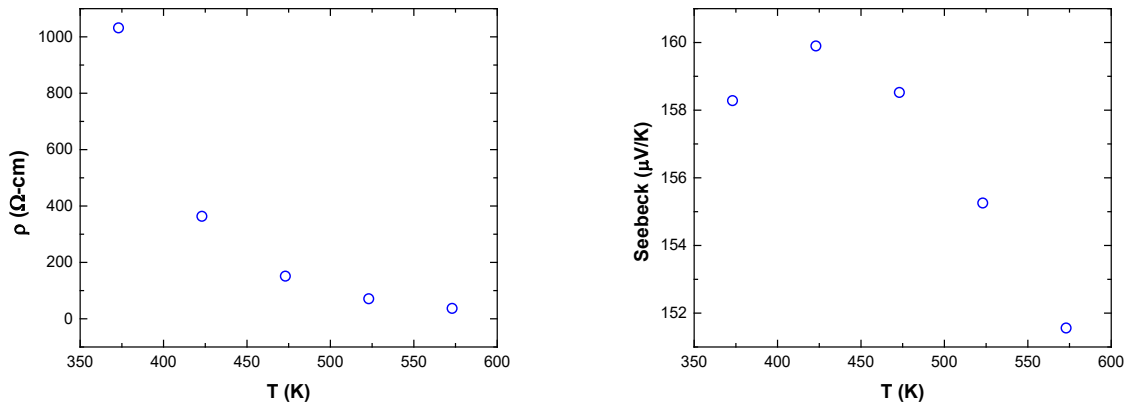
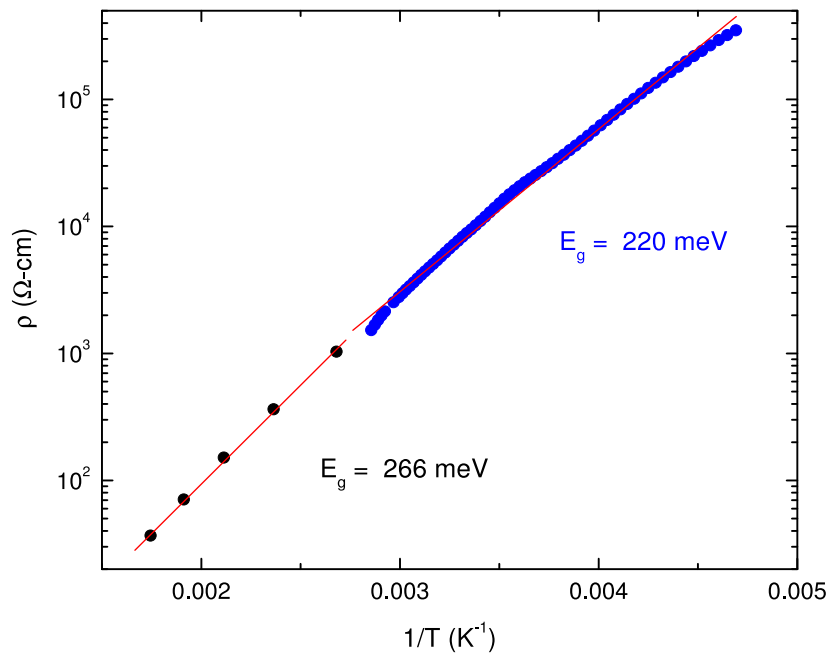**Figure 5.** High temperature resistivity (left) and Seebeck coefficient data (right) of $Li_{2.15}Os_{0.85}O_3$ sample from 350 to 600 K.

Figure 6. Resistivity versus temperature for $Li_{2.15}Os_{0.85}O_3$ in the range 200 – 600 K versus inverse temperature. The low and high temperature measurements were performed in different apparatuses on samples from the same growth run. To assure continuity at T = 300K, the data have been rescaled for the low temperature measurement due to its greater uncertainty in the geometric factor.
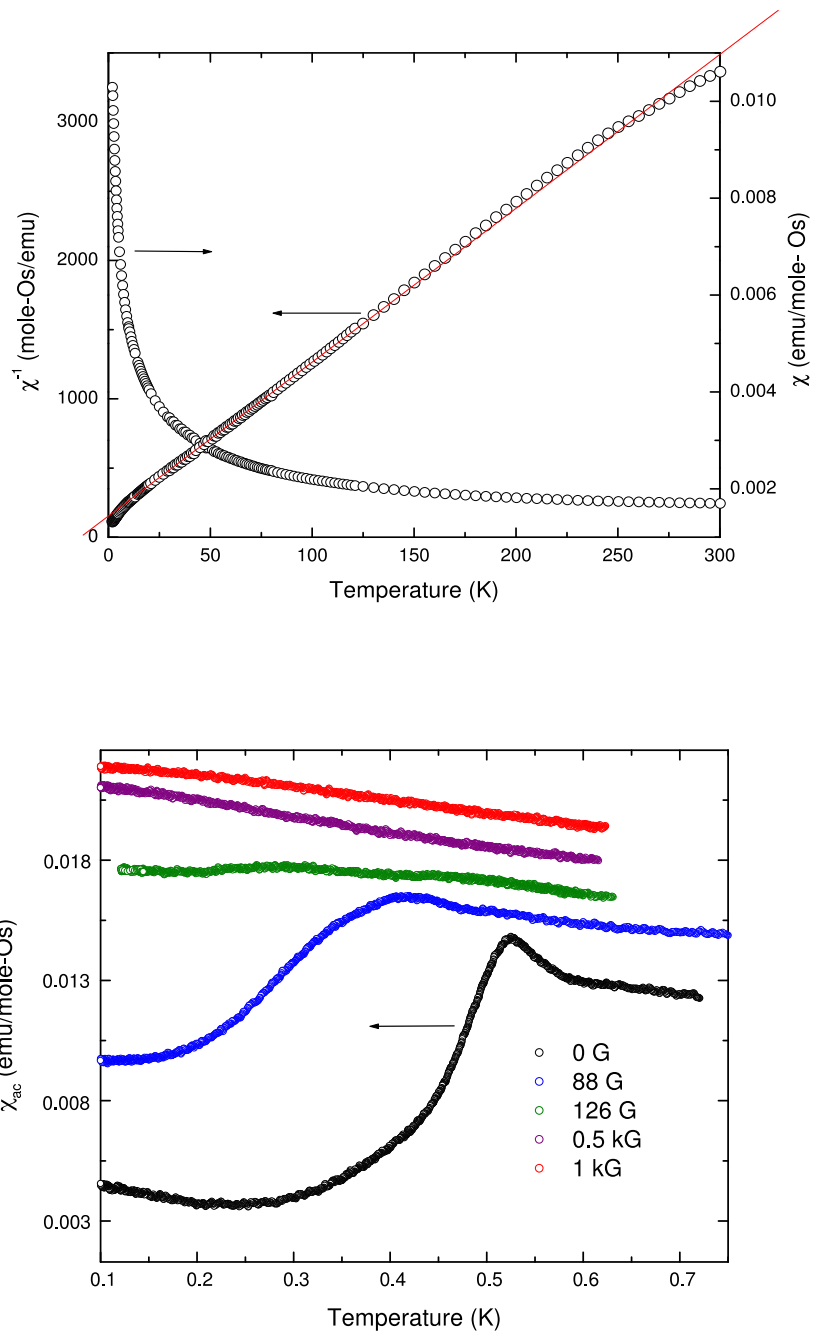
Figure 7. Top: DC-Susceptibility $Li_{2.15}Os_{0.85}O_3$ versus temperature. Also shown is the inverse susceptibility after subtracting a van Vleck term as described in the text. Bottom: ac-susceptibility versus temperature at different values of applied magnetic field. The curves have been offset vertically by 0.0020, 0.0032, 0.0044, and 0.0056 emu for H = 88, 126, 500, and 1000G respectively, for clarity.
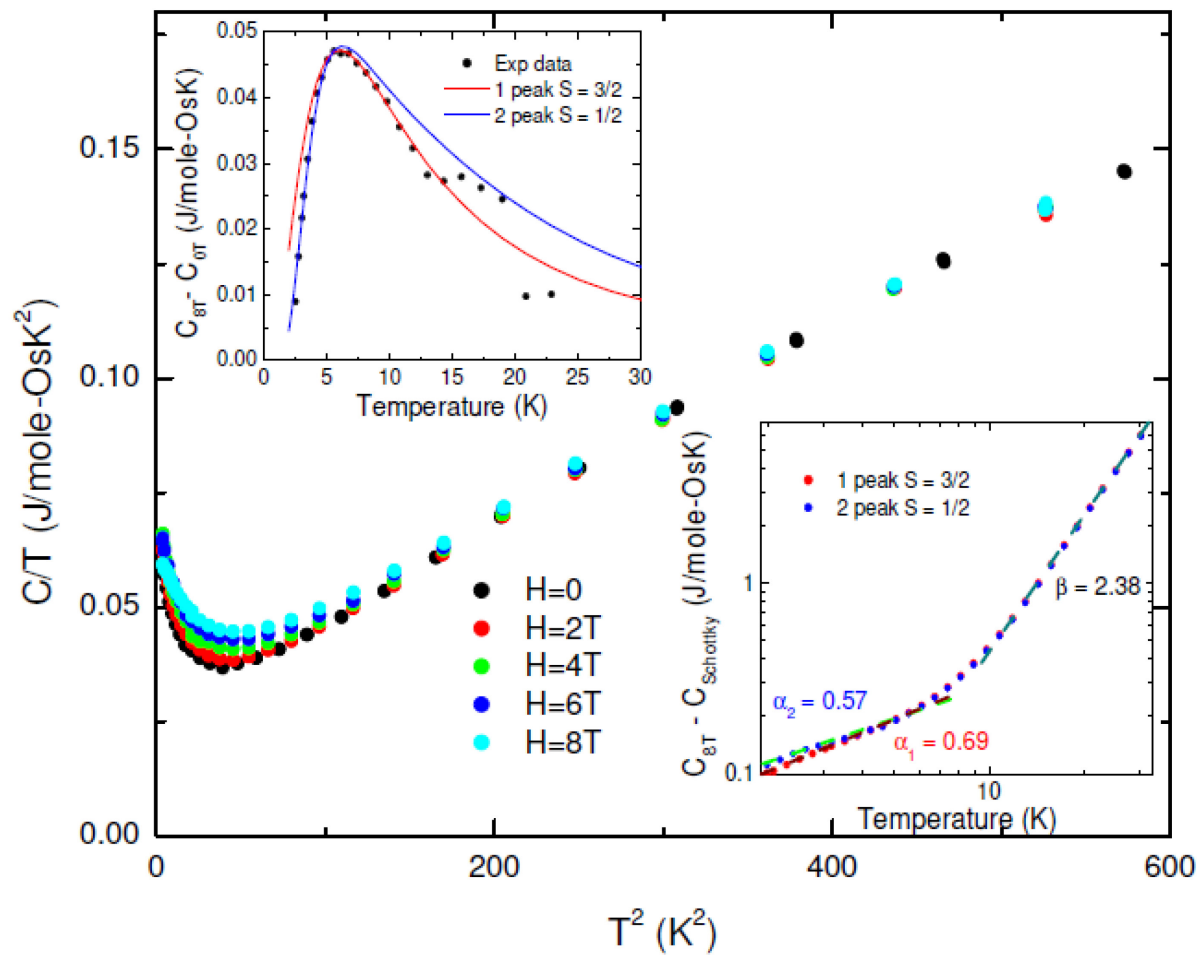
Figure 8. The specific heat C(T) of Li_2OsO_3 in various applied fields, measured using a Physical Property Measurement System. Upper Inset: Impurity spins modeled with a Schottky anomaly. Lower Inset: Specific heat after removing the impurity contribution.
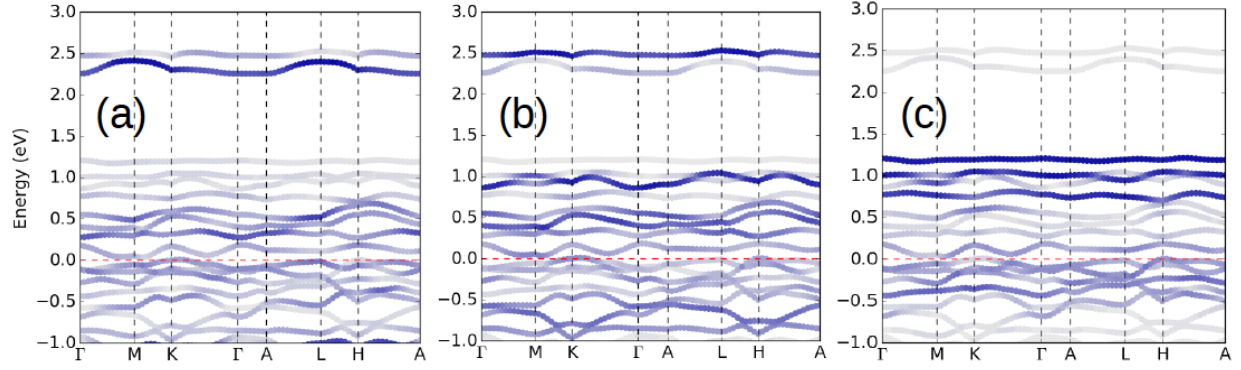
Figure 9. Plot of bands in the Os t_{2g} region of 25% Li-substituted Li_2OsO_3 on the Os honeycomb sublattice, with energy zero (horizontal red line) denoting the gap region. The fatbands plots emphasize the Os 5d character on (a) the Os[0] site with no Li neighbor, (b) the Os[1] site with one Li neighbor, and (c) the Os[2] site with two Li neighbors. While Os[0] and Os[1] show some differences, Os[2] is qualitatively different.

References

1. G. Khaliullin, Excitonic Magnetism in Van Vleck-type d^4 Mott Insulators, *Physical Review Letters*, **111**, 197201, (2013).
2. Alexei Kitaev, Anyons in an exactly solved model and beyond, *Annals of Physics*, **321**, 2-111, (2006).
3. I. Felner, I.M. Bradarić, The magnetic behavior of Li_2MO_3 (M = Mn, Ru and Ir) and $Li_2(Mn_{1-x}Ru_x)O_3$, Phys. B Condens. Matter. 311 (2002) 195–199.
4. James, A.C.W.P.; Goodenough, J.B.; Structure and bonding in Li_2MoO_3 and $Li_{2-x}MoO_3$ ($0 \leq x \leq 1.7$), J. Solid State Chem. 76 (1988) 87–96.
5. Sinha, A.; Nair, S.R.; Sinha, P.K., Single step synthesis of Li_2TiO_3 powder, J. Nucl. Mater. 399 (2010) 162–166.
6. Pantyukhina, M.I.; Obrosov, V.P.; Stepanov, A.P.; Study of Ion Transport in Li_2ZrO_3 Solid Electrolytes with Different Lithium Isotope Ratios, Crystallogr. Reports. 49 (2004) 676–679.
7. J. Breger, M. Jiang, N. Dupre, Y.S. Meng, Y. Shao-Horn, G. Ceder, et al., High-resolution X-ray diffraction, DIFFaX, NMR and first principles study of disorder in the Li_2MnO_3–$Li[Ni_{1/2}Mn_{1/2}]O_2$ solid solution, J. Solid State Chem. 178 (2005) 2575–2585.
8. W. Schmidt, R. Berthelot, L. Etienne, A. Wattiaux, M.A. Subramanian, Synthesis and characterization of O3-$Na_3LiFeSbO_6$: A new honeycomb ordered layered oxide, Mater. Res. Bull. 50 (2014) 292–296.
9. Z. Lu, J.R. Dahn, Effects of Stacking Fault Defects on the X-ray Diffraction Patterns of T_2 , O_2 , and O_6 Structure $Li_{2/3}[Co_xNi_{1/3-x}Mn_{2/3}]O_2$, Chem. 13 (2001) 2078–2083.
10. Torres-Castro, Loraine; Abreu-Sepulveda, Maria A.; Katiyar, Ram S.; Manivannan, A., Electrochemical Investigations on the Effect of Mg-Substitution in Li2MnO3 Cathode, Journal of the Electrochemical Society (2017), 164(7), A1464-A1473.
11. Abbasian, A. R.; Rahimipour, M. R.; Hamnabard, Z., Hydrothermal Synthesis of Lithium Meta Titanate Nanocrystallites, Procedia Materials Science (2015), 11, 336-341.
12. Manni, S.; Choi, I.I.; Mazin, R.; Coldea, H.O.; Jeschke, R.; Valenti, Effect of isoelectronic doping on honeycomb lattice iridate A_2IrO_3, Phys. Rev. B., 89 (2014) 245113 (1-7).
13. Singh, Y.; Gegenwart, P., Antiferromagnetic Mott insulating state in single crystals of the honeycomb lattice material, Phys. Rev. B., 82 (2010) 1–7.
14. Mccalla, E., Abakumov, A.M.; Foix, D.; Berg, E.J.; Rousse, G.; Doublet, M., Visualization of O-O peroxo-like dimers in high-capacity layered oxides for Li-ion batteries, Science 350 (2015) 1516–1521.
15. S. Okada, J. Yamaki, K. Asakura, H. Ohtsuka, H. Arai, S. Tobishima, et al., Cathode characteristics of layered rocksalt oxide, Li_2PtO_3, Electrochim. Acta. 45 (1999) 329–334.
16. Baklanova, Y.V.; Ishchenko, A.V.; Denisova, T.A.; Maksimova, L.G.; Shulgin, B.V.; Pustovarov, V.A., Photo- and radioluminescence of lithium hafnate Li_2HfO_3, Opt. Mater. (Amst). 34 (2012) 1037–1041.
17. Kobayashi, H.; Tabuchi, M.; Shikano, M.; Kageyama, H.; Kanno, R., Structure, and magnetic and electrochemical properties of layered oxides, Li_2IrO_3, J. Mater. Chem. 13 (2003) 957–962.
18. Sandhya Kumari, L.; Wallace, M.; Barnes, J.T.; Tong, B.; Ramirez, A.P.; Subramanian, M.A; Charge transfer instability in a mixed Ir/Rh honeycomb lattice in Li2Ir1-xRhxO3 solid solution; Solid State Sciences (2016), 61, 232-238.
19. Singh, Y. et al. Relevance of the Heisenberg-Kitaev model for the honeycomb lattice

iridates A2IrO3; Phys. Rev. Lett. 108, 127203 (2012).

20. Singh, Y., & Gegenwart, P. Antiferromagnetic Mott insulating state in single crystals of the honeycomb lattice material, Na2IrO3; Phys. Rev. B 82, 064412 (2010).

21. T. Takayama, A. Kato, R. Dinnebier, J. Nuss, H. Takagi; Hyper-honeycomb iridate β-Li2IrO3 as a platform for Kitaev magnetism; Phys. Rev. Lett. 114, 077202 (2015).

22. Banerjee et al., Neutron scattering in the proximate quantum spin liquid a-RuCl3; Science 356, 1055–1059, (2017).

23. A.P. Ramirez, Strongly Geometrically Frustrated Magnets, Ann. Rev, Mater. Sci. Vol 24, 453 -80 (1994)

24. A.R. Makintosh and O. K. Andersen, in Electrons at the Fermi Surface, p. 149 ed. M. Springford, Cambridge Univ. Press (1980)

25. L.S.I. Veiga et al., Fragility of ferromagnetic double exchange interactions and pressure tuning of magnetism in 3d−5d double perovskite Sr2FeOsO6, Physical Review B 91, 235135 (2015)

26. Heiba, Z.K.;El Sayed, K.; J. Appl. Cryst., (2002), 35, 634-636

27. Jansen, V.; Hoppe, R., Z.;Zur Kenntnis der NaCl-Strukturfamilie: Neue Untersuchungen an Li2MnO3; Anorg. Allg. Chem., (1973), 397, 279.

28. Boulineau, A.; Croguennec, L., et. al.,;Reinvestigation of Li2MnO3 Structure: Electron Diffraction and HighResolution TEM; Chem. Mater., 21, 4216-4222 (2009).

29. Hibble, S.J.; Fawcett, I.D.; Hannon, A.C.; Acta Cryst. (1997). B53, 604-612.

30. M.J. O'Malley, H. Verweij, P.M. Woodward, J. Solid State Chem. 181 (2008), 1803-1809.

31. O'Malley, M.J., Woodward, P.M., A Structural, Bonding, and Properties Study of the Ordered Rock Salt Structures, Li_2MO_3 (M = Ru, Ir, Pt), Dissertation Thesis, Ohio State University, (2009).

32. Katukuri, V. M. et al. Strong magnetic frustration and anti-site disorder causing spin-glass behavior in honeycomb Li2RhO3. Sci. Rep. 5, 14718; doi: 10.1038/srep 14718 (2015).

33. H. Lei, W. Yin, Z. Zhong, H. Hosono, Phys. Rev. B 89 (1-5) (2014) 020409.

34. G. van der Laan and B. T. Thole, Phys Rev Lett 60, 1977 (1988)

35. M.A. Laguna-Marco et al. PRL 105, 216407 (2010)

36. S. Gangopadhyay and W. E. Pickett, Spin-orbit coupling, strong correlation, and insulator-metal transitions: the J_{eff}=1/2 ferromagnetic Dirac-Mott insulator Ba2NaOsO6 , Phys. Rev. B 91, 045133 (2015).

37. S. Gangopadhyay and W. E. Pickett, Interplay between spin-orbit coupling and strong correlation effects: Comparison of the three osmate double perovskites Ba2AOsO6 (A=Na, Ca, Y), Phys. Rev. B 93, 155126 (2016).

38. I. I. Mazin, H. O. Jeschke, K. Foyevtsova, R. Valentí, and D. I. Khomskii, Na2IrO3 as a Molecular Orbital Crystal, Phys. Rev. Lett. 109, 197201 (2012).

39. Y. Singh, S. Manni, J. Reuther, T. Berlijn, R. Thomale, W. Ku, S. Trebst, and P. Gegenwart, Relevance of the Heisenberg-Kitaev Model for the Honeycomb Lattice Iridates A_2IrO_3, Phys. Rev. Lett. **108**, 127203 (2012).

40. I. I. Mazin, S. Manni, K. Foyevtsova, H. O. Jeschke, P. Gegenwart, and R. Valenti, Phys. Rev. B **88**, 035115 (2013).

41. Y. Yamaji, Y. Nomura, M. Kurita, R. Arita, and M. Imada, First-Principles Study of the Honeycomb-Lattice Iridates Na_2IrO_3 in the Presence of Strong Spin0Orbit Interaction and Electronic Correlations, Phys. Rev. Lett. **113**, 107201 (2014).

42. S.. Nishimoto, V. M. Katururi, V. Ysuhankhai, H. Stoll, U. K. Roessler, L. Hozoi, I. Rousochatzakis, and J. van den Brink, Strongly frustrated triangular spin lattice emerging from triplet dimer formation in honeycomb Li2IrO3, Nat. Commun.

DOI:10.1038/ncomms10273.

43. K. Hu, F. Wang, and J. Feng, First-Principles Study of the Magnetic Structure of Na2IrO3, Phys. Rev. Lett. 115, 167204 (2015).

44. M. Kim, B. H. Kim. And B. I. Min, Insulating nature of Na2IrO3: Mott-type oor Slater-type, Phys. Rev. B 93, 195135 (2016).

45. Y. Li, S. M. Winter, H. O. Jeschke, and R. Valenti, Electronic excitations in gamma-Li2IrO3, Phys. Rev. B 95, 045129 (2017).

46. X. Gonze et al., ABINIT: first-principles approach to materials and nanosystem properties, Comp. Phys. Commun. 180, 2582 (2009).

47. D. C. Wallace; T. M. McQueen; Dalton Trans.; (2015); 44, 20344–20351.

48. D. C. Wallace, C. M. Brown; T. M. McQueen; J. Solid State Chem.; (2015); 224, 28–35.

49. Bette, S., et. al.; Dalton Trans.; (2017); 46; 15216.

50. X. Gonze et al., Recent developments in the ABINIT software package, Computer Phys. Comm. 205, 106 (2016).

51. Perdew, J. P.; Burke, K.; Ernzerhof, M. Generalized GradientApproximation Made Simple. Phys. Rev. Lett. 1996, 77, 3865.

52. M. Torrent, F. Jollet, F. Bottin, G. Zerah, and X. Gonze, Implementation of the Projector Augmented-Wave Method in the ABINIT code, Comput. Mat. Science 42, 337, (2008).

53. B. Amadon, F. Jollet and M. Torrent, Gamma and beta cerium: LDA+U calculations of ground-state parameters.Phys. Rev. B 77, 155104 (2008).

54. See for example D. D. O'Regna and G. Teobaldi, Optimization of constrained density functional theory, Phys. Rev. 94, 035159 (2016) and references therein.